SEMARAK ILMU PUBLISHING

Journal of Advanced Research in Fluid Mechanics and Thermal Sciences

Journal homepage:
https://semarakilmu.com.my/journals/index.php/fluid_mechanics_thermal_sciences/index
ISSN: 2289-7879

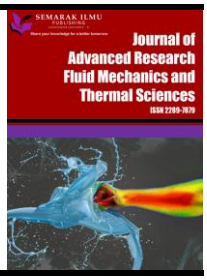

Two-phase Upward Flow-Induced Vibrations in U-bend under Different Orientations

Muhammad Sohail[1], William Pao[1,*], Huzaifa Azam[1], Umair Khan[1]

[1] Mechanical Engineering Department, Universiti Teknologi PETRONAS (UTP), Seri Iskandar 32610, Perak, Malaysia

ARTICLE INFO

Article history:
Received 8 October 2023
Received in revised form 24 December 2023
Accepted 3 January 2024
Available online 15 February 2024

Keywords:
U-bend; orientation; multiphase; fluid structure interaction; air-water; vibrations

ABSTRACT

U-bends are frequently employed in industries to change the direction of fluid flow. Flow Induced Vibrations (FIV) are very prominent due to internal two-phase flow and vary with U-bend orientation. Potential possibilities of spatial orientations of a U-bend make it impractical to predict these vibrations using an experimental approach. This study investigates the two-phase flow-induced vibrations for 0°, 30°, 60° and 90° upward flow in a U-bend using CFD. In-plane and out-of-plane directional vibrational data was gathered for these four orientations of U-bend. For constant superficial velocities with void fraction of 0.5, impact of orientation on slug frequencies was observed with Fast Fourier Transformation. In-plane (x-axis) forces applied at the outlet bend significantly increase 39% compared to the corresponding forces at the inlet bend. Forces at the outlet bend along the y-axis (out-of-plane) were reduced by 26%, but the forces along the z-axis show a more moderate decrease of 7%. This study provides significant data essential to forming a correlation of two-phase flow-induced vibrations with multiple upward flow U-bend orientations.

1. Introduction

Flow Induced Vibrations (FIV) occur frequently in U-bends with internal two-phase flow [1]. These vibrations can cause severe damage and subsequently, fatigue failures leading to safety concerns [2]. Predicting these vibrations is crucial to achieve a sustainable and efficient business operation [3]. Orientation of the flow conduit is a major factor contributing to FIV [4]. With many possibilities of U-bends' orientations for upward flow, it is economically not viable to perform experimental investigation. Two-phase flow creates various flow patterns depending on flow characteristics, geometric properties, inclination of flow conduit, mechanical properties of fluids and surface roughness [5,6]. Flow regime pattern has a significant impact on fluid behavior at bends. Common flow regimes depending on the void fraction of phases in two-phase flow are bubbly, slug, churn, and annular flow [7,8].

* *Corresponding author.*
E-mail address: william.pao@utp.edu.my

https://doi.org/10.37934/arfmts.114.1.112

Annular and slug flows were found to have the largest pressure drop amplitudes in U-bend. Power Spectral Density (PSD) showed reduction in slug flow frequency but increase in annular flow frequency for reversed flow from downward to upward in U-bend [9]. This indicates substantial dependence of vibrations on momentum flux at bends. Superficial velocities, pressure fluctuation, flow regimes and relative gas-liquid flow properties are some of the influencing factors defining the amplitude and frequency of FIV. Numerical and experimental studies performed for horizontal and vertical upward two-phase flow provided typical flow regime maps to generate various flow regimes with superficial velocities [10-12].

Theoretical investigations were carried out for impact of superficial velocities and film thickness on pressure drop in two-phase flow [13]. However, these studies did not focus their investigation on elbows as U-bend consists of two 90° elbows. This could be due to difficulties in handling complex geometry analytically. Abrupt curved shape of elbows generates sufficient Coriolis forces resulting in significant pressure drop between the inner and outer curvature radii [14]. Pressure drops in 90^{o} bends caused by variation in curvature radius was studied for upward two-phase flow [15]. They concluded that as much as 25% loss in pressure is possible. Factors such as pipeline pressure profiles, pressure in real time, and liquid holdup were discovered to identify pressure drop at bends [15]. In the situation of U-bend, it becomes even more complicated to extract the correlation between flow regime and pressure drop. Flow regimes are transformed at bends and mostly stay in intermittence state between the elbows in U-bend [9,16]. Orientation of the flow channel plays a very important role in dynamic responses of the structure. An inclined pipeline-riser system was investigated experimentally and numerically for severe slugging [17]. Wide range of elastic foundation vibrations, shearing forces and bending moment at bends were observed. They also indicated the vulnerable spots at bends because of severe slugging flow.

Contemporarily, there is a missing technical gap for correlation of internal two-phase flow induced vibrations in U-bends upward flow with respect to orientations. Based on current industrial practices, investigating vibrations and peak pressure fluctuations in U-bends with different orientations require separate experiments or CFD simulations for each variation [17]. Additionally, two-phase flow in U-bends structure can lead to complex flow dynamics, making it challenging to accurately predict directional pressure fluctuations [18-21]. By investigating U-bends of constant diameter, curvature ratio (R/D), U-bend lengths and phase superficial velocities with variable angular positions, this study provides a comprehensive understanding of orientations impact on U-bend vibrations.

2. Methodology

2.1 Geometry

U-bend geometry used in this research had inlet and outlet arm of 1.5 m length with bend arm length of 0.5 m. Flow channel had internal diameter of 3 inches and radius to diameter ratio for each bend as 1. Figure 1(a) shows three straight fluid bodies that are inlet arm, outlet arm and bend arm along with inlet and outlet bends. Phasic volume fraction prescribed at inlet boundary of flow channel cross section is shown in Figure 1(b).

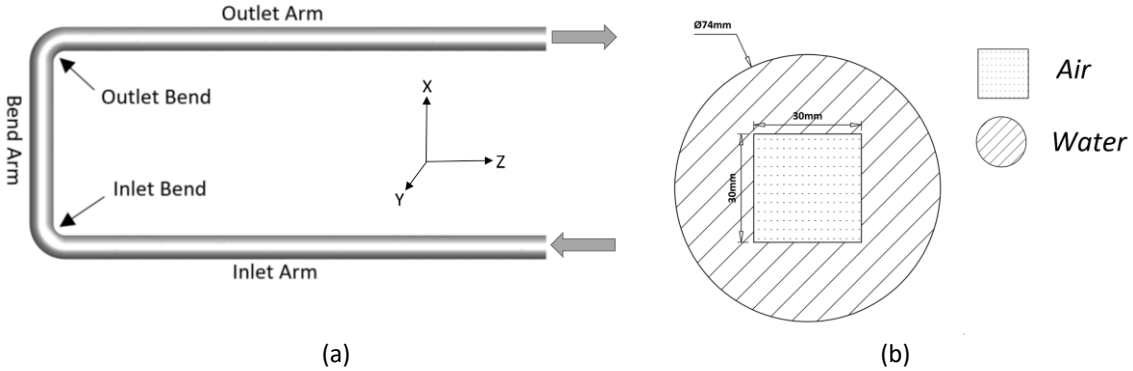

(a) (b)

Fig. 1. U-bend geometry (a)U-bend arms and bends, (b) Inlet surface cross sections

Directional deflections experienced by each bend for a duration of 5 seconds were recorded. Impulsive momentum change occurred at bends which created maximum pressure drop and thus was the optimal location for data collection.

2.2 Mesh Independence Study

Turbulency in two-phase flow increases with inclination angle of the U-bend [22]. Hence a single fixed mesh generated for horizontal flow is not appropriate for upward flow. Mesh independence study was carried out separately for $0°$ (horizontal flow) and $90°$ (vertically upward flow) U-bend geometric orientations for this study are shown in Figure 2. This examination is crucial for ensuring precision in computations, offering insights into the distinct requirements posed by both extreme horizontal and vertically upward flows of U-bend orientations.

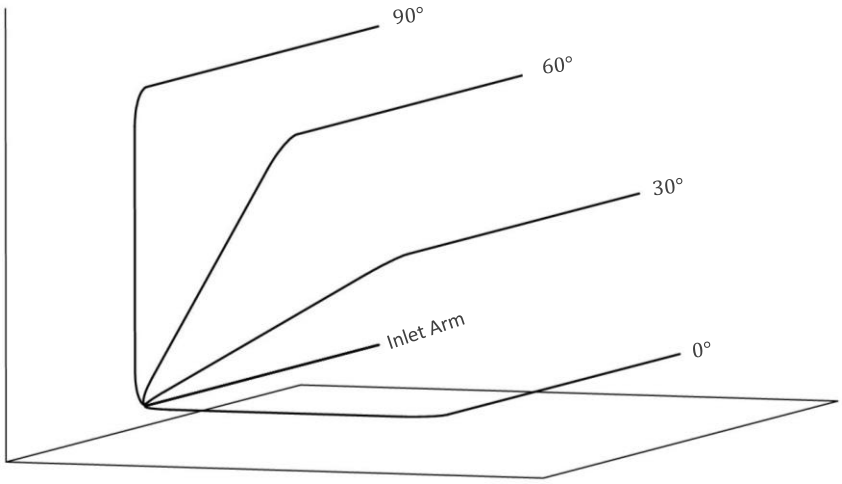

Fig. 2. Horizontal to vertically upward flow U-bend orientations

2.2.1 Orientation based flow mesh convergence

Flow in U-bend was horizontal when the gravity acted perpendicular to U-bend plane (X, Z) as shown in Figure 1(a). Flow was vertically upward when gravity acted in negative X direction. To avoid computational instability, element size was selected for tessellation keeping the Courant number below 0.5. Longitudinal flow in inlet and outlet arms stayed perpendicular to gravity while rotating U-bend from horizontal to vertically upward flow. Fixed mesh body size of 7 mm was selected for inlet and outlet arm [23]. The element size of Inlet bend, outlet bend, and bend arm were varied to

find number of elements that converge mesh independence study curves. Calculations for the expected number of elements were carried out to satisfy the computation limitations. The simulation model geometry is intricately divided into five components: Inlet Arm, Inlet Bend, Bend Arm, Outlet Bend, and Outlet Arm, as delineated in Table 1. To determine the anticipated number of elements for each section, the volume occupied by fluid within the geometry is calculated and divided by the corresponding element size. This approach ensures a tailored meshing strategy, allowing for precise and efficient simulations of individual U-bend components. The element count increased from 97,847 to 240,912 employing four mesh densities with element sizes of 3.75 mm, 3 mm, 2.75 mm, and 2.5 mm. Table 1 and Table 2 show approximate number of elements calculated for four cases of mesh independence study under consideration.

Table 1
U-bend segregated mesh elements calculation based on element size

Geometry	Volume (m^3)	Element Size (mm)	Number of Elements
Inlet arm	0.00645	7	18,805
Inlet bend	0.0005133	3.75	9,734
		3	19,011
		2.75	24,682
		2.5	32,851
Bend arm	0.00215	3.75	40,770
		3	79,630
		2.75	103,381
		2.5	137,600
Outlet bend	0.0005133	3.75	9,734
		3	19,011
		2.75	24,682
		2.5	32,851
Outlet arm	0.00645	7	18,805

Table 2
Approximate number of elements for each case of Mesh Independence Study

Geometry	Case_01	Case_02	Case_03	Case_04
Inlet arm	18,805	18,805	18,805	18,805
Inlet bend	9,734	19,011	24,682	32,851
Bend arm	40,770	79,630	103,381	137,600
Outlet bend	9,734	19,011	24,682	32,851
Outlet arm	18,805	18,805	18,805	18,805
Total Number of Elements	97,847	155,261	190,353	240,912

The complex interactions between meshing details in the simulation model are depicted in the Figure 3. It provides a visual representation of the actual number of elements encountered in each mesh independence study instance. Case_01 to Case_04 correspond to mesh configurations with 98,956, 152,325, 195,232, and 243,692 elements, respectively. This illustration represents the dynamic complexities inherent in the meshing procedure. It also highlights subtle variation caused by bend features and the careful balancing of mesh elements.

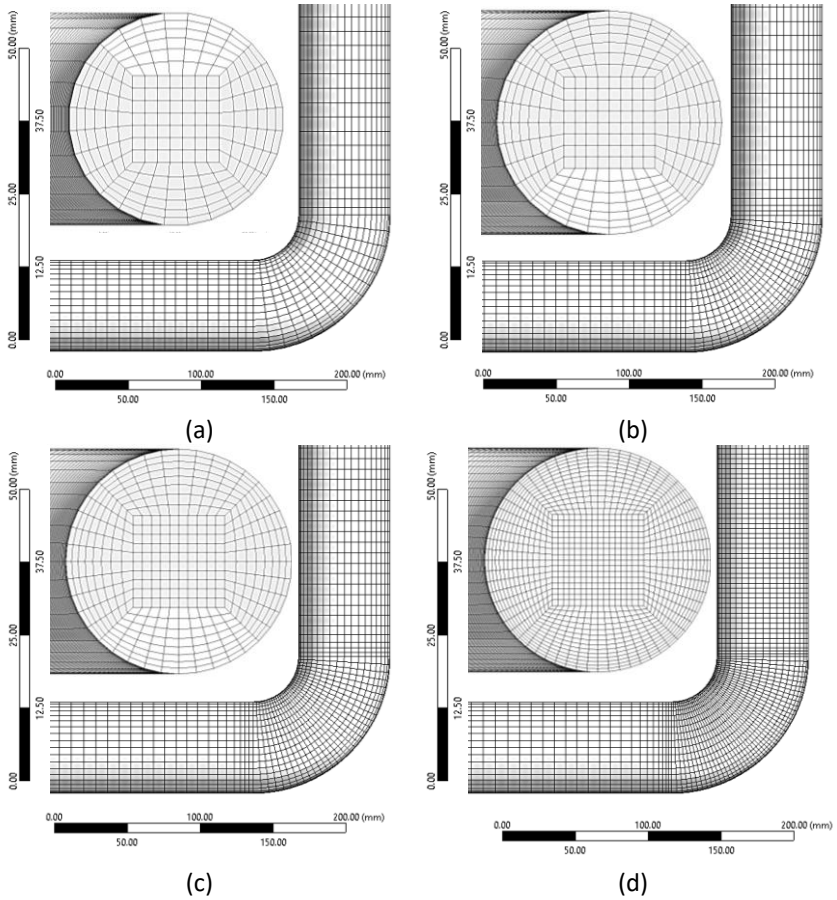

Fig. 3. Mesh number of elements selection (a) 98956 elements, (b) 152325 elements, (c) 195232 elements, (d) 243692 elements

The suitable number of elements for horizontal flow was 150,000 but vertically upward flow curve had steep variations at this number of elements. The appropriate number of elements, 195,232, were used to achieve the dynamic pressure curve convergence for both extreme orientations of this study and shown in Figure 4.

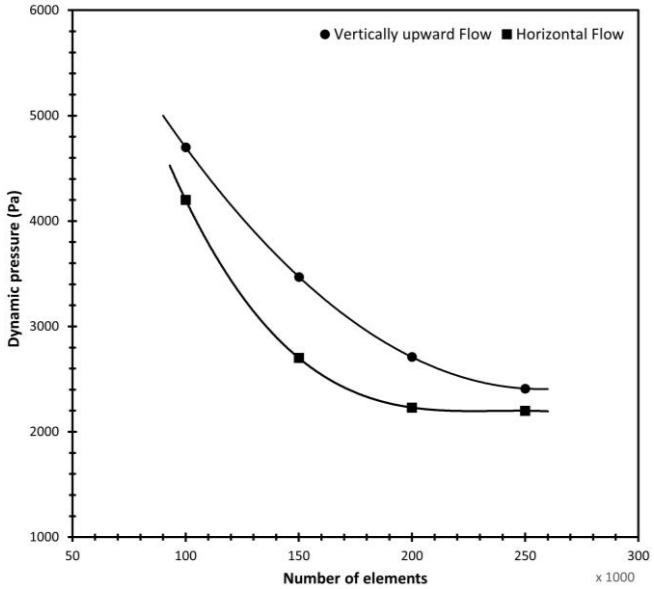

Fig. 4. Mesh Convergence Study for 0° Horizontal and 90° Vertically Upward Flow

2.3 Boundary Conditions

Superficial phasic velocities were prescribed at the inlet boundary shown in Figure 1(b) according to their respective volume fraction. Inlet vector velocities were configured orthogonal to the inlet cross section. Selected superficial velocities of this study maintained void fraction around 0.5 within the flow channel [24]. According to the inlet surface area ratio, superficial velocity of water and air were fixed at 1.02 m/s and 3.865 m/s respectively. The outlet boundary of U-bend was set with atmospheric pressure. Pipe inner-surface was set to fluid solid interface and fluid outer-surface was set to wall boundary with dynamic mesh for two-way coupling. A constant 0.072 N/m inter-phasal surface tension was prescribed for air and water with densities of 1.225 $\mathrm{kg/m^3}$ and 998.2 $\mathrm{kg/m^3}$ respectively. Pipe structure of the model was constrained at both ends with fixed support condition (all 6 degree of freedoms were fixed).

2.4 CFD Model

Volume of Fluid (VOF) pressure-based CFD solver with coupled algorithm was used to solve the system of momentum and pressure-based continuity equations simultaneously [25]. Continuity and momentum equations for this model are shown in Eq. (1) and Eq. (2), respectively.

$$\frac{\partial \rho}{\partial t} + \nabla \cdot (\rho \vec{v}) = 0 \tag{1}$$

$$\frac{\partial \rho}{\partial t}(\rho \vec{v}) + \nabla \cdot (\rho \vec{v} \vec{v}) = -\nabla \mathrm{p} + \nabla \cdot [\mu(\nabla \vec{v} + \nabla \vec{v}^T)] + \rho \vec{g} + \vec{F} \tag{2}$$

Continuity equation ensures the conservation of fluid mass in a control volume over time. ρ is the fluid density, $\vec{v}$ is the fluid velocity at time t of fluid flow. Momentum equation shows the conserved momentum of fluid in a control volume with respect to time. In this equation p represents the fluid pressure, fluid viscosity is given by μ. Term $\nabla\mu(\nabla\vec{v})$ accounts for the viscous stress tensor having $\nabla\vec{v}$ gradient of fluid velocity. $\vec{g}$ is the gravitational acceleration vector and $\vec{F}$ are other external forces applied. Turbulence modeling $k - \varepsilon$ was used for this study [26]. Equations for turbulence kinetic energy and its dissipation are stated as Eq. (3) and Eq. (4).

$$\frac{\partial (\rho k)}{\partial t} + \nabla \cdot (\rho k \vec{v}) = \nabla \left[\left(\mu + \frac{\mu_t}{\sigma_k} \right) \nabla k \right] + G_k + G_b - \rho \varepsilon - Y_m + S_k \tag{3}$$

$$\frac{\partial (\rho \varepsilon)}{\partial t} + \nabla \cdot (\rho \varepsilon \vec{v}) = \nabla \left[\left(\mu + \frac{\mu_t}{\sigma_\varepsilon} \right) \nabla \varepsilon \right] + C_{1\varepsilon} \frac{\varepsilon}{k} (G_k + C_{3\varepsilon} G_b) - C_{2\varepsilon} \rho \frac{\varepsilon^2}{k} + S_\varepsilon \tag{4}$$

G_k and G_b indicate turbulence kinetic energy generated due to mean velocity gradients and buoyancy respectively. Contribution of fluctuating dilation to overall dissipation rate is represented by Y_M, while having $C_{i\varepsilon}$ as constants. Turbulent Prandtl numbers for k and ε are σ_k and σ_ε respectively. User-defined source terms are given by S_k and S_ε [24]. Volume fraction of gas α_g and liquid α_l can be computed using Eq. (5) and Eq. (6), respectively.

$$\frac{\partial \alpha_g}{\partial t} + \vec{v} \cdot \nabla \alpha_g = 0 \tag{5}$$

$$\alpha_l = 1 - \alpha_g \tag{6}$$

2.5 Data Collection

CFD simulations were carried out for $0°$, $30°, 60°$ and $90°$ with two-way coupled U-bend. Maximum pressure fluctuations and structural deformations for flow induced vibrations analysis were observed at both elbows of the U-bend [27]. Three-dimensional deformations experienced at inlet and outlet bend were recorded for the simulation time of 2-5 seconds. Directional Vibrations in x and z-axis are in-plane while y-axis is out-of-plane motion for this U-bend as shown in Figure 1. Deformation in x, y, and z-axis for all four orientations were processed and transformed to frequency domain. Variation in frequency and vibrational amplitude with orientations were analyzed to form relationship of orientation with vibration in U-bend.

3. Results and Discussion

Two-phase flow pressure dropped as the flow passes through the bends. Figure 5 shows CFD contour results performed for $0°$ horizontal flow orientation. Velocity selected for this study produced annular flow across the inlet arm. From pressure contours it was evident that the initial pressure at section (a) was higher and gradually distributed across the cross section of the pipe with maximum pressure at the center. Annular flow regime pressure distribution had maximum pressure at the center because of higher gas superficial velocity while lower pressures exist at the periphery of the flow channel. Pressure is immensely dropped at between section (b) and (c) and minimum pressure was observed at section (d).

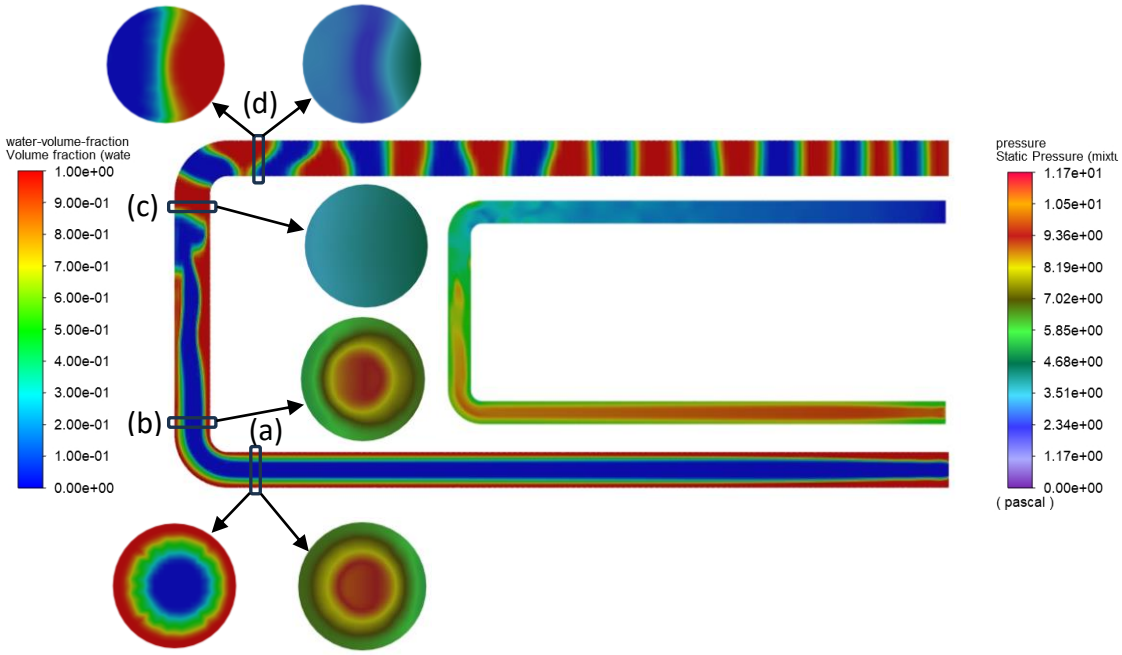

Fig. 5. Annular flow, water volume fraction and pressure drop for horizontal flow

Flow transitions are observed with varying angular position of U-bend. Figure 6 shows flow contours for 0^o, 30^o, 60^o, and 90^o. As the inclination increased, the flow in the bend arm tends more towards annular. In the case of a 90-degree orientation, annular flow was observed in the bend arm. The water volume fraction of the outlet arm for $0°$ shows a similar contour to that of $90°$, while the outlet arms for $30°$ and $60°$ show a more consistent water volume fraction transition.

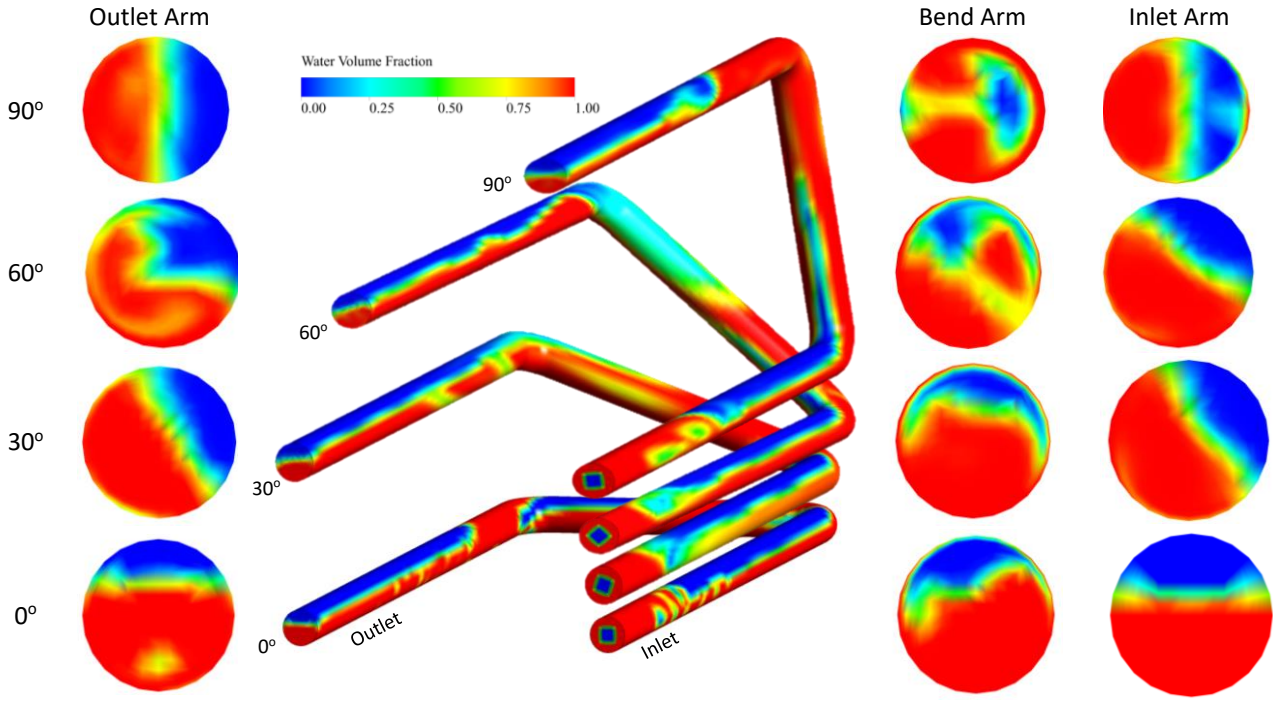

Fig. 6. Water volume fraction Flow transition for 0°, 30°, 60° and 90° vertical upward flow

Pressure drop is observed for horizontal flow in Figure 5, as it passes through inlet bend, bend arm and outlet bend. Impact at bends is recorded to study the influence of annular flow compared to other flow regimes created in inclined U-bend. It was observed that the outlet bends experiences more force than the inlet bends as annular flow increases based on pressure contours of these inclinations. Impact forces percentage difference analysis is carried out in Figure 9 to display this behavior.

As a result of variation in pressure drop with orientation of the U-bend, directional deformation and applied forces on bends surfaces were collected and transformed using Fast Fourier Transformation. FFT plots for directional deformation of inlet and outlet bends in x, y, and z-axis were plotted for 0°, 30°, 60° and 90° orientations shown in Figure 2. Figure 7(a) and Figure 7(b) shows the x-axis (in-plane) deformation frequencies for inlet and outlet bend respectively. Frequencies in x-axis observed are 7.87 and 8 hertz for all four orientations. Frequencies below 10 Hz are considered very dangerous in fluid industry, however it has high dependence on the superficial velocities. Amplitude of x-axis frequencies decreased from 0° to 60° and was increased again for 90° orientation. From Figure 7(b) and Figure 7(e), there was a secondary y-axis (out-of-plane) peak frequency observed. Peak frequencies observed in y-axis were 6.37, 6.67 and 15.67 Hz.

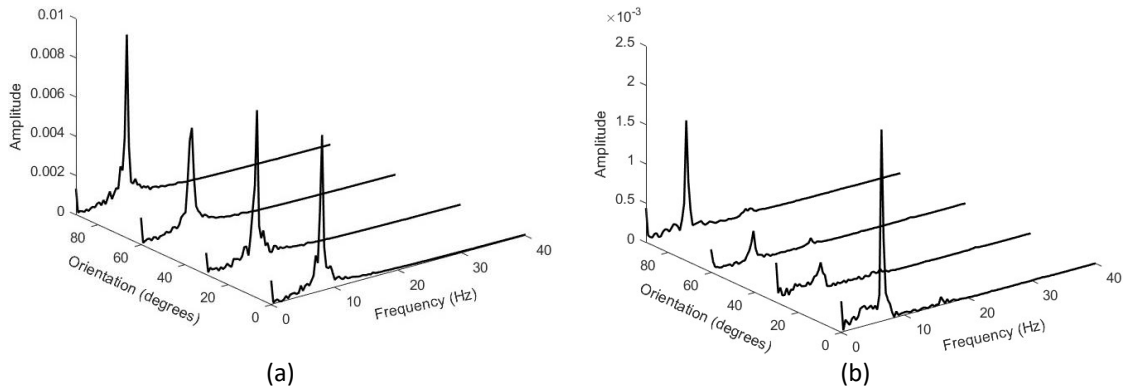

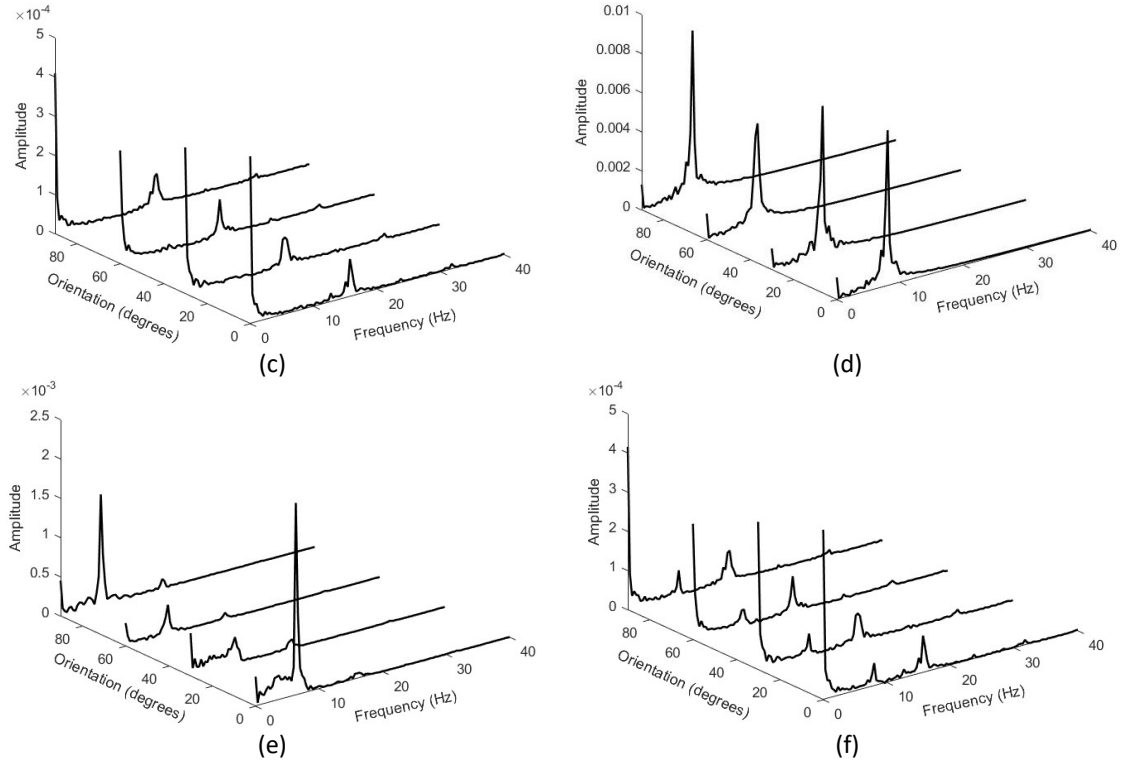

Fig. 7. Fast Fourier Transformed frequencies of inlet and outlet bend directional deflections (a) x-axis deformation FFT of inlet bend, (b) y-axis deformation FFT of inlet bend, (c) z-axis deformation FFT of inlet bend, (d) x-axis deformation FFT of outlet bend, (e) y-axis deformation FFT of outlet bend, (f) z-axis deformation FFT of outlet bend

Single deflection peak frequency was observed in z-axis (in-plane) for inlet bend while outlet bend had 7.87, 15.74 and 15.667 hertz as peak frequencies for $0°, 30°, 60°$ and $90°$ orientations. Forces applied on structure bends surfaces were recorded and FFT plots were generated for directional fluctuations in each bend as shown in Figure 8.

Applied forces on the bends surface shown in Figure 8, had at least two peak fluctuations. However, peak deflection was observed because of single peak upon comparison with Figure 7. Only z-axis (in-plane) deformation in outlet bend had two frequency peaks. The first peak is of 8 Hz while the second peak frequency was found to be around 15 Hz. The first peak frequency is because of the vibration in x-axis which is the primary axis of in-plane vibration. This observation is crucial as the secondary peak forces give rise to deflection in secondary directions.

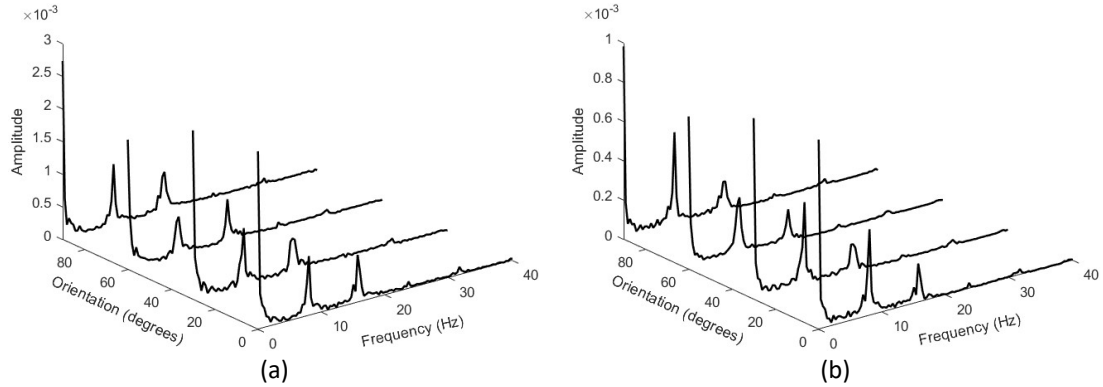

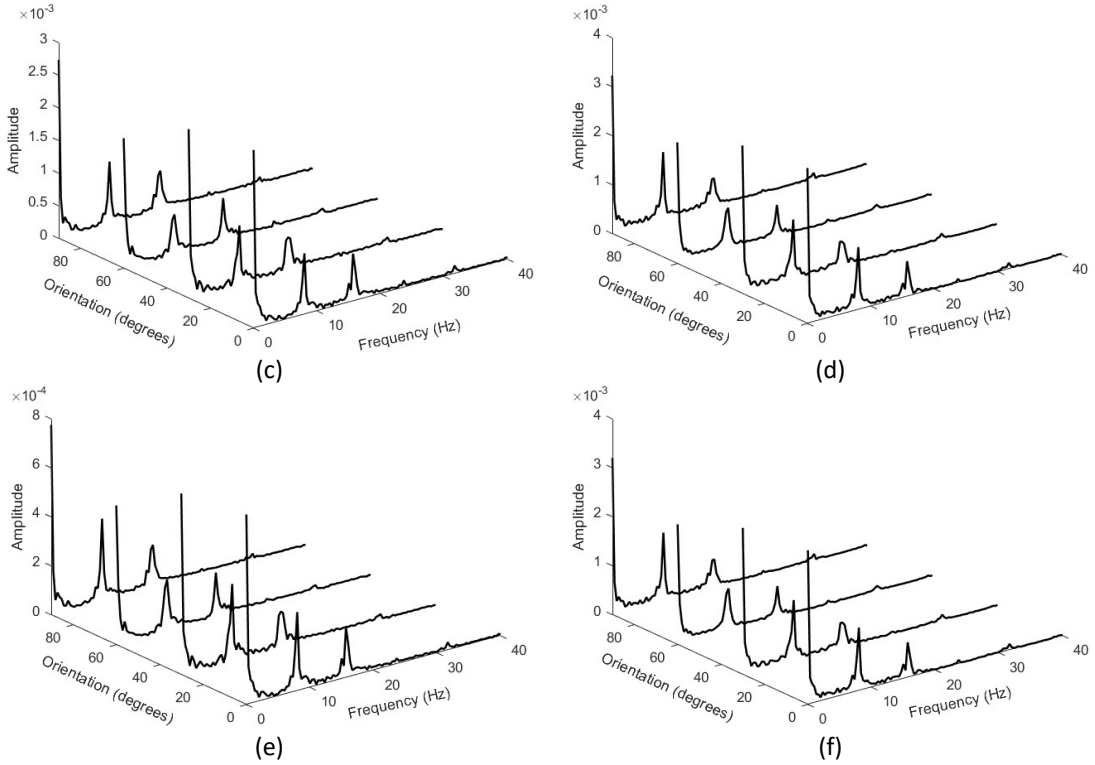

Fig. 8. Force fluctuations FFT for inlet and outlet bend (a) x-axis force fluctuation on inlet bend, (b) y-axis force fluctuation on inlet bend, (c) z-axis force fluctuation on inlet bend, (d) x-axis force fluctuation on outlet bend, (e) y-axis force fluctuation on outlet bend, (f) z-axis force fluctuation on outlet bend

Directional forces applied at the inlet bend were compared with corresponding directional forces at the outlet bend for $0°, 30°, 60°$ and $90°$ orientations. Percentage difference for x, y and z-axis forces of outlet and inlet bend is shown in Figure 9.

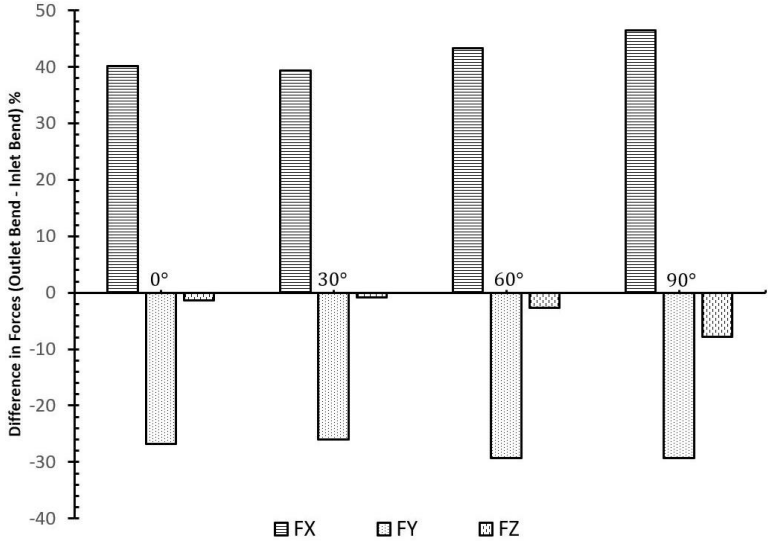

Fig. 9. Percentage difference of directional forces between inlet and outlet bend for upward flow orientations

Consistent variations in applied forces amplitude were observed at bends for varying orientation. Amplitudes were decreased by 3% in x and y-axis while 28% reduction in amplitude was observed in z-axis for change in orientation from $0°$ to $30°$. From $30°$ to $60°$, x and y-axis vibrational amplitude was reduced further by 32% but 25% increase was observed for z-axis. Changing orientation from $60°$ to $90°$, x and y-axis experienced an increase in amplitude by 60% while z-axis amplitude was reduced by 12%.

4. Conclusions

Force applied at the inlet and outlet bends varied with change in U-bend orientation. Similar behaviour was shown by direction deformation produced for in-plane and out-of-plane motion. Peak vibrational frequencies for in-plane (x, z-axis) vibration were in the range of 7-8 Hz and 14-16 Hz. Peak frequencies observed in y-axis (out-of-plane) were 6.37, 6.67 and 15.67 Hz. These frequencies were also confirmed by force fluctuations applied on bends surfaces. Flow regime transition from stratified to annular flow was observed while changing orientation from 0^o horizontal position to 90^o vertically upward flow. This flow pattern transition resulted in increased impact forces at the outlet bend with increase in upward flow angular position. In-plane (x-axis) forces applied at the outlet bend show a significant increase of 39% when compared to those experienced at the corresponding inlet bend. The forces applied at the outlet bend along the y-axis (out-of-plane) were reduced by 26%, but the forces along the z-axis show a more moderate decrease of 7%. Impact of orientation on directional vibrations along with relation between forces applied on each is formed in this study.

Acknowledgement

The authors would like to acknowledge the financial support from the Universiti Teknologi PETRONAS Institute of Contaminant Management via the Graduate Assistantship scheme and Universiti Teknologi PETRONAS Foundation via YUTP Fundamental Research Grant.

References

[1] Haile, Samuel Gebremariam, Elmar Woschke, Getachew Shunki Tibba, and Vivek Pandey. "Internal two-phase flow induced vibrations: A review." *Cogent Engineering* 9, no. 1 (2022): 2083472. https://doi.org/10.1080/23311916.2022.2083472

[2] Zheng, X., Z. Wang, M. S. Triantafyllou, and G. E. Karniadakis. "Fluid-structure interactions in a flexible pipe conveying two-phase flow." *International Journal of Multiphase Flow* 141 (2021): 103667. https://doi.org/10.1016/j.ijmultiphaseflow.2021.103667

[3] Reza, Shah Danial Shah, and Mohammad Rasidi Rasani. "Vibrations of a vertical 90° pipe bend under two-phase flow conditions." *International Journal of Structural Integrity* 13, no. 6 (2022): 885-906. https://doi.org/10.1108/IJSI-03-2022-0028

[4] Bamidele, Olufemi E., Wael H. Ahmed, and Marwan Hassan. "Two-phase flow induced vibration of piping structure with flow restricting orifices." *International Journal of Multiphase Flow* 113 (2019): 59-70. https://doi.org/10.1016/j.ijmultiphaseflow.2019.01.002

[5] Jia, Wei, and Brian McPherson. "Multiphase Flow Associated With Geological CO_2 Storage." In *Science of Carbon Storage in Deep Saline Formations*, pp. 117-143. Elsevier, 2019. https://doi.org/10.1016/B978-0-12-812752-0.00006-X

[6] Khan, Umair, William Pao, and Nabihah Sallih. "A review: Factors affecting internal two-phase flow-induced vibrations." *Applied Sciences* 12, no. 17 (2022): 8406. https://doi.org/10.3390/app12178406

[7] Klinkenberg, Arnout M., and Arris S. Tijsseling. "Stochastic mechanistic modelling of two-phase slug flow forces on bends in horizontal piping." *International Journal of Multiphase Flow* 144 (2021): 103778. https://doi.org/10.1016/j.ijmultiphaseflow.2021.103778

[8] Shin, Hong-Cheol, and Sung-Min Kim. "Experimental investigation of two-phase flow regimes in rectangular micro-channel with two mixer types." *Chemical Engineering Journal* 448 (2022): 137581. https://doi.org/10.1016/j.cej.2022.137581

[9] Ma, Xiaoxu, Maocheng Tian, Jingzhi Zhang, Liangliang Tang, and Furen Liu. "Flow pattern identification for two-phase flow in a U-bend and its contiguous straight tubes." *Experimental Thermal and Fluid Science* 93 (2018): 218-234. https://doi.org/10.1016/j.expthermflusci.2017.12.024
[10] Mandhane, J. M., G. A. Gregory, and K. Aziz. "A flow pattern map for gas-liquid flow in horizontal pipes." *International Journal of Multiphase Flow* 1, no. 4 (1974): 537-553. https://doi.org/10.1016/0301-9322(74)90006-8
[11] Li, Kun, Qiang Wang, and Mi Wang. "Three-dimensional visualisation of gas-water two-phase flow based on bubble mapping method and size projection algorithm." *Flow Measurement and Instrumentation* 69 (2019): 101590. https://doi.org/10.1016/j.flowmeasinst.2019.101590
[12] Ullah, Atta, Hamzah Sakidin, Shehza Gul, Kamal Shah, Yaman Hamed, Maggie Aphane, and Thabet Abdeljawad. "Sensitivity analysis-based control strategies of a mathematical model for reducing marijuana smoking." *AIMS Bioengineering* 10, no. 4 (2023): 491-510. https://doi.org/10.3934/bioeng.2023028
[13] Chen, Hu, Shuo Liu, Jian Zhang, and Jing-Yu Xu. "Oil-water two-phase flow-induced vibration of a cylindrical cyclone with vortex finder." *Physics of Fluids* 35, no. 4 (2023). https://doi.org/10.1063/5.0140066
[14] Li, Yalin, Xikun Wang, Shouqi Yuan, and Soon Keat Tan. "Flow development in curved rectangular ducts with continuously varying curvature." *Experimental Thermal and Fluid Science* 75 (2016): 1-15. https://doi.org/10.1016/j.expthermflusci.2016.01.012
[15] Spedding, P. L., and Emmanuel Bénard. "Gas-liquid two phase flow through a vertical 90 elbow bend." *Experimental Thermal and Fluid Science* 31, no. 7 (2007): 761-769. https://doi.org/10.1016/j.expthermflusci.2006.08.003
[16] Wang, Lin, Yiren Yang, Chang Liu, Yuxing Li, and Qihui Hu. "Numerical investigation of dynamic response of a pipeline-riser system caused by severe slugging flow." *International Journal of Pressure Vessels and Piping* 159 (2018): 15-27. https://doi.org/10.1016/j.ijpvp.2017.11.002
[17] Lima, Ricardo J. Da Silva, and John R. Thome. "Two-phase flow patterns in U-bends and their contiguous straight tubes for different orientations, tube and bend diameters." *International Journal of Refrigeration* 35, no. 5 (2012): 1439-1454. https://doi.org/10.1016/j.ijrefrig.2012.02.002
[18] Matsui, Goichi. "Automatic identification of flow regimes in vertical two-phase flow using differential pressure fluctuations." *Nuclear Engineering and Design* 95 (1986): 221-231. https://doi.org/10.1016/0029-5493(86)90049-X
[19] Vieira, Saon Crispim, Charlie van der Geest, Adriano Todorovic Fabro, Marcelo Souza de Castro, and Antonio Carlos Bannwart. "Intermittent slug flow identification and characterization from pressure signature." *Mechanical Systems and Signal Processing* 148 (2021): 107148. https://doi.org/10.1016/j.ymssp.2020.107148
[20] Marode, Roshan Vijay, Srinivasa Rao Pedapati, Tamiru Alemu Lemma, and Mokhtar Awang. "A review on numerical modelling techniques in friction stir processing: current and future perspective." *Archives of Civil and Mechanical Engineering* 23, no. 3 (2023): 154. https://doi.org/10.1007/s43452-023-00688-6
[21] Ullah, Atta, Hamzah Sakidin, Shehza Gul, Kamal Shah, Mohana Sundaram Muthuvalu, Thabet Abdeljawad, and Mudassar Iqbal. "Sensitivity analysis-based validation of the modified NERA model for improved performance." *Journal of Advanced Research in Applied Sciences and Engineering Technology* 32, no. 3 (2023): 1-11. https://doi.org/10.37934/araset.32.3.111
[22] Vakamalla, Teja Reddy, Kedar S. Kumbhar, Ravi Gujjula, and Narasimha Mangadoddy. "Computational and experimental study of the effect of inclination on hydrocyclone performance." *Separation and Purification Technology* 138 (2014): 104-117. https://doi.org/10.1016/j.seppur.2014.10.013
[23] Khan, Umair, William Pao, and Nabihah Sallih. "Numerical Gas-Liquid Two-Phase Flow Regime Identification in a Horizontal Pipe Using Dynamic Pressure Data." *Applied Sciences* 13, no. 2 (2023): 1225. https://doi.org/10.3390/app13021225
[24] Khan, Umair, William Pao, Nabihah Sallih, and Farruk Hassan. "Identification of Horizontal Gas-Liquid Two-Phase Flow Regime Using Deep Learning." *CFD Letters* 14, no. 10 (2022): 68-78. https://doi.org/10.37934/cfdl.14.10.6878
[25] El Ouafa, Simon, Stéphane Vincent, Vincent Le Chenadec, and Benoît Trouette. "Fully-coupled parallel solver for the simulation of two-phase incompressible flows." *Computers & Fluids* 265 (2023): 105995. https://doi.org/10.1016/j.compfluid.2023.105995
[26] Adanta, Dendy, IM Rizwanul Fattah, and Nura Muaz Muhammad. "Comparison of standard k-epsilon and SST k-omega turbulence model for breastshot waterwheel simulation." *Journal of Mechanical Science and Engineering* 7, no. 2 (2020): 39-44. https://doi.org/10.36706/jmse.v7i2.44
[27] Zhou, Mengmeng, Shibo Kuang, Fei Xiao, Kun Luo, and Aibing Yu. "CFD-DEM analysis of hydraulic conveying bends: Interaction between pipe orientation and flow regime." *Powder Technology* 392 (2021): 619-631. https://doi.org/10.1016/j.powtec.2021.07.052